# Optical spectra of single-wall carbon nanotube bundles

M. F. Lin
*Department of Physics, National Cheng Kung University, Tainan, Taiwan 701, The Republic of China*
(Received 24 April 2000)

The low-frequency optical properties of single-wall carbon nanotube bundles are studied within the gradient approximation. The nanotube geometry (diameter and chiral angle) and the polarization direction strongly affect the optical absorption function, the dielectric function, the loss function, and the reflectance. The low-frequency absorption spectra in the $\mathbf{E}_{\|}$ case clearly exhibit three absorption bands. The semiconducting (metallic) nanotubes induce the first and the second absorption bands (the third absorption band). Subpeaks, which come from the single-particle excitations of the band-edge states, exist in each absorption band. They could be used to determine the preferred nanotube geometry in a single-walled nanotube bundle. Similar results are obtained for the dielectric function and the reflectance spectra. However, the loss spectra could exhibit the prominent peaks due to the inter-$\pi$-band plasmons. They are not useful in determining the distribution of diameter and chiral angle. The inter-$\pi$-band plasmons also lead to clear plasmon edges in the reflectance spectra. The calculated results could essentially explain the measured absorption spectra and loss spectra.

## I. INTRODUCTION

A class of quasi-one-dimensional (1D) systems, carbon nanotubes, was discovered by Iijima[1] in 1991. A single-wall carbon nanotube is a rolled-up graphite sheet in the cylindrical form. It is a semiconductor or a metal, which depends on both diameter and chirality.[2–7] The $\pi$ band formed by $2p_z$ orbitals is very special. A single-wall carbon nanotube has many 1D parabolic subbands except that the subbands nearest the Fermi level ($E_F=0$) in a metallic nanotube are linear, i.e., all subbands have divergent density of states (DOS) in $1/\sqrt{E}$ form except the finite DOS of the linear subbands. The 1D van Hove singularities (vHS's) in the DOS have a strong effect on many solid-state properties, such as the absorption spectrum, loss spectrum, and reflectance spectrum. When single-wall carbon nanotubes are closely packed together, a 3D carbon nanotube bundle is formed.[8] Single-wall carbon nanotubes might differ in diameter and chirality. The distribution of diameter and chiral angle is significantly affected by catalysts[9,10] and synthesis temperature.[11] x-ray diffraction,[8] optical absorption,[9,10] Raman spectroscopy,[11,12] electron diffraction,[12,13] and transmission electron spectroscopy[14] have been used to characterize the nanotube geometry. Single-wall carbon nanotubes in a bundle are found to comprise largely nanotubes of armchair chirality. In this work, we study the low-frequency optical properties ($<$2.5 eV) of single-wall carbon nanotube bundles, including optical absorption function, dielectric function, loss function, and reflectance. Their dependence on the distribution of diameter and chiral angle and on the polarization direction of an external electric field is investigated. Comparison with recent measurements is discussed.[9,10,15]

The optical absorption spectra of single-wall carbon nanotube bundles were measured by photothermal deflection spectroscopy.[9] Three absorption bands, which come from the electron-hole ($e$-$h$) excitations, appear at low frequency $\omega$ $<$2 eV. The first two absorption bands and the third absorption band are identified from the semiconducting and the metallic carbon nanotubes, respectively. More detailed absorption spectra[10] show that there are several subpeaks in each absorption band. The energy positions of the subpeaks are equidistantly separated on the diameter scale with the almost same value $d_c/2\simeq 0.07$ nm. This length is just one-half of the diameter difference between two neighboring armchair carbon nanotubes (Sec. II). Moreover, the peak positions are insensitive to changes in the synthesis temperature. These two results imply that the diameters of single-wall nanotubes are grouped around a preferred value, and the chiralities of single-wall carbon nanotubes are close to the armchair chirality. Electron-energy-loss spectroscopy[15] (EELS) was used to measure the loss function of single-wall carbon nanotube bundles. There are prominent peaks in the loss spectrum at small transferred momentum. They are identified as the inter-$\pi$-band collective excitations (plasmons). This work will investigate the relation between peaks in loss spectra and those in absorption spectra.

We use the tight-binding model to calculate the $\pi$ band of a single-wall carbon nanotube. A detailed description of the low-energy $\pi$ band is found to be very important in understanding the optical spectra. The $\pi$ bands are very different for carbon nanotubes close to armchair chirality and zigzag chirality, and so do the optical spectra. As a result of the 1D vHS, there are many peak structures in absorption spectrum, dielectric function, reflectance spectrum, and loss spectrum. The prominent peaks in loss spectrum contrast greatly with the peak structures in the absorption spectrum and reflectance spectrum. In addition to peak structures, the reflectance spectrum exhibits clear plasmon edges. The calculated results could explain the experimental measurements.[9,10,15]

This paper is organized as follows. The low-energy $\pi$ band is calculated in Sec. II. The gradient approximation[16] is used to evaluate the optical absorption function, dielectric function, loss function, and reflectance. The calculated optical spectra are discussed in Sec. III. Finally, Sec. IV contains the concluding remarks.

## II. LOW-FREQUENCY OPTICAL EXCITATIONS

The geometric and electronic structures of carbon nanotubes are simply reviewed. As has been discussed,[17] a single-

 

wall carbon nanotube is a rolled-up graphite sheet, the structure of which is thus fully specified by a 2D lattice vector $\mathbf{R}_x = m\mathbf{a}_1 + n\mathbf{a}_2$, where $\mathbf{a}_1$ and $\mathbf{a}_2$ are primitive lattice vectors of a graphite sheet. The diameter and the chiral angle of a $(m,n)$ carbon nanotube are $d = |\mathbf{R}_x|/\pi = b\sqrt{3(m^2+mn+n^2)}/\pi$ $(b = 1.42\,\text{Å})$ and $\theta = \tan^{-1}[-\sqrt{3}n/(2m+n)]$, respectively. Carbon nanotubes close to the (9,9) armchair nanotube $(-30° \leqslant \theta \leqslant -20°)$ or the (15,0) zigzag nanotube $(-10° \leqslant \theta \leqslant 0°)$ are chosen for a model study.

The electronic structure of the $(m,n)$ carbon nanotube is calculated within the tight-binding model, which is similar to that employed for a graphite sheet.[18] The $\pi$-band structure of a graphite sheet is caused by the overlapping carbon $2p_z$ orbitals, which belong to two sublattices. The Hamiltonian in the subspace spanned by the two tight-binding functions $U_1(k_x,k_y)$ and $U_2(k_x,k_y)$ is thus described by a $2\times 2$ matrix

$$H = \begin{pmatrix} 0 & H_{12}(k_x,k_y) \\ H_{12}^*(k_x,k_y) & 0 \end{pmatrix}, \tag{1}$$

where $H_{12}(k_x,k_y) = -\gamma_0 \Sigma_{i=1}^{3} e^{-i\mathbf{k}\cdot\mathbf{r}_i}$. The Hamiltonian only contains the interactions of each carbon atom with its three nearest neighbors, denoted by $\mathbf{r}_i$. $\gamma_0$ is the resonance integral. $\mathbf{k}$ is the Bloch wave vector, and $k_x$ is parallel to $\mathbf{R}_x$.

The Bloch states of Eq. (1), when applied to a carbon nanotube, must satisfy the periodical boundary condition $\psi(\mathbf{r}) = \psi(\mathbf{r}+\mathbf{R}_x)$. The $\pi$-band energy dispersions of the $(m,n)$ nanotube are obtained from diagonalizing the Hamiltonian:

$$E^{c,v}(k_x,k_y) = \pm\gamma_0\Bigg[1 + 4\cos\left(\frac{3b(k_y\cos\theta + k_x\sin\theta)}{2}\right)\cos\left(\frac{\sqrt{3}b(k_y\sin\theta - k_x\cos\theta)}{2}\right) + 4\cos^2\left(\frac{\sqrt{3}b(k_y\sin\theta - k_x\cos\theta)}{2}\right)\Bigg]^{1/2}, \tag{2a}$$

and the wave functions are

$$\Psi^{c,v}(k_x,k_y) = \frac{1}{\sqrt{2}}\left(U_1(k_x,k_y) \mp \frac{H_{12}^*(k_x,k_y)}{|H_{12}(k_x,k_y)|}U_2(k_x,k_y)\right). \tag{2b}$$

The transverse wave vector $k_x = 2J/d$, and the axial wave vector $k_y$ is confined within the first Brillouin zone. $J = 1,2,...,N_u/2$, where $N_u$ is the atom number in a unit cell. The quantized angular momentum $J$ serves as the subband index. The superscript $c(v)$ represents the antibonding $\pi^*$ band (the bonding $\pi$ band). The Fermi energy is equal to zero, and electrons only occupy the bonding $\pi$ band at $T = 0$. From Eq. (2a), a carbon nanotube with $2m+n = 3I$ $(\neq 3I$; $I$ is an integer) is a gapless metal (a moderate-gap semiconductor). The diameter difference between two neighboring metallic nanotubes is defined as the characteristic length. $d_c$ is equal to $3b/\pi = 0.14\,\text{nm}$ $(3\sqrt{3}b/\pi = 0.23\,\text{nm})$ for armchair (zigzag) carbon nanotubes.

An analytic form is derived for the low-energy $\pi$ band. It is important in explaining the main features of the low-frequency optical excitations. The $\pi$-band states of a carbon nanotube are sampled from those of a graphite sheet; that is, they are derived from the states inside the hexagonal Brillouin zone (BZ).[17] The states near the corner [the $K$ point in Fig. 2(b) of Ref. 17] correspond to the low-energy states of a carbon nanotube. The $K$ point is located at $(4\pi/3\sqrt{3}b)(\cos\theta, -\sin\theta)$. By expanding the energy dispersions in Eq. (2a) about the $K$ point, the low-energy $\pi$ band is described by

$$E^{c,v}(\kappa_x,\kappa_y) = \pm\gamma_0\Bigg(\frac{9b^2}{4}[\kappa_x^2+\kappa_y^2] + \frac{9b^3\kappa_x}{8}[\kappa_x^2 - 3\kappa_y^2]\cos 3\theta + \frac{9b^3\kappa_y}{8}[\kappa_y^2 - 3\kappa_x^2]\sin 3\theta - \frac{27b^4}{64}[\kappa_x^2+\kappa_y^2]^2\Bigg)^{1/2}. \tag{3}$$

$\kappa_x = (2/d)(j - i/3)$, where $j = 0, \pm 1, \pm 2, ...$, and $i$ satisfies $2m+n = 3I - i$. $\kappa_x = 0, \mp 2/d, \pm 4/d, \ldots$ for a metallic carbon nanotube with $i = 0$, and $\kappa_x = -2/3d, 4/3d, \ldots (2/3d, -4/3d, \ldots)$ for a semiconducting carbon nanotube with $i = 1(-1)$. The $\kappa_y = 0$ edge state leads to the 1D vHS in the DOS. Its energy depends on the $\kappa_x^2$ and $\kappa_x^3\cos 3\theta$ terms in Eq. (3). The latter is relatively important for carbon nanotubes with small $\theta$. Equation (3) is suitable only for the states close to the subband edge. However, this equation is very useful in understanding the low-energy $\pi$ band. For example, it could be used to determine the energy positions of the 1D vHS.

How the nanotube geometry affects the low-energy $\pi$ band deserves a detailed investigation. The joint density of states (JDOS) is defined as

$$D_J(\omega) \sum_J \int_{1\text{st BZ}} \frac{dk_y}{2\pi}\frac{\Gamma}{[\omega - 2E^c(J,k_y)]^2 + \Gamma^2}, \tag{4}$$

where $\Gamma (= 0.005\gamma_0)$ is a phenomenological level broadening parameter. The JDOS at $\omega$ is simply one-half of the DOS of the $\pi^*$ bands at $E^c = \omega/2$. It is proportional to the optical absorption function [Eq. (5)] for the parallel polarization $(\mathbf{E}_\parallel \| \hat{y})$. Figure 1(a) shows the JDOS for the metallic carbon nanotubes of approximately the same diameter $(d \sim 1.15-1.29\,\text{nm})$. The linear subbands of $\kappa_x = 0$ [Eq. (3)] induce a finite JDOS at low frequency $(\omega < 0.6\gamma_0)$. The higher-energy subband, with $\kappa_x = 2/d$ or $-2/d$, has a parabolic energy dispersion. The JDOS due to the $\kappa_y = 0$ edge state diverges in $1/\sqrt{\omega - \omega_3}$ form at $\Gamma = 0$, i.e., it exhibits 1D vHS's. At small $\Gamma$, the divergent structure is replaced by a sharp peak. The $\pi^*$ subband of $\kappa_x = -2/d$ is lower than that of $\kappa_x = 2/d$ [the $\kappa_x^3$ term in Eq. (3)]. These two subbands are not degenerate except for the $(m,m)$ armchair nanotubes. The nonarmchair metallic nanotubes thus exhibit two neighboring peaks. Their energy positions, $\omega_{3a}$ and $\omega_{3b}$, depend on diameter and chiral angle. $\omega_{3a}$ and $\omega_{3b}$ could be obtained from the $\kappa_a^2$ and $\kappa_x^3\cos 3\theta$ terms in Eq. (3). The energy dif-

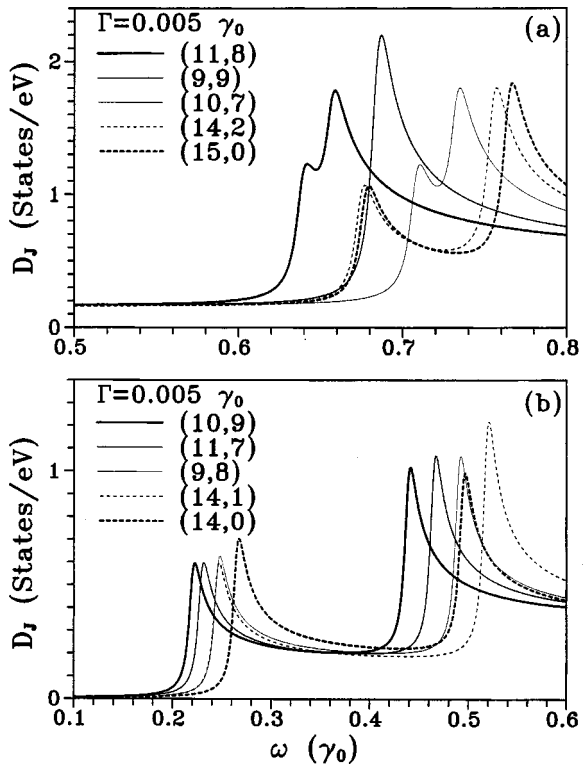


FIG. 1. The joint density of states is shown at $\Gamma=0.005\gamma_0$ for (a) the metallic nanotubes and (b) the semiconducting nanotubes. The unit of frequency is $\gamma_0$.

ference between these two prominent peaks, $E_D=\omega_{3b}-\omega_{3a}=6\gamma_0 b^2\cos 3\theta/d^2$, decreases with chiral angle. $E_D$ is a maximum for a $(m,0)$ zigzag nanotube $\theta=0°$, and it is zero for a $(m,m)$ armchair nanotube with $\theta=-30°$. The two neighboring peaks are expected to be relatively easily observed for metallic carbon nanotubes close to zigzag chirality. There is no simple rule between the energy position of the first peak and the nanotube diameter. That the $\kappa_x^3\cos 3\theta$ term in Eq. (3) is not negligible is the main reason. For example, the (9,9) nanotube is larger than the (15,0) nanotube, while the first peak of the former exhibits at higher energy. But for metallic carbon nanotubes with close chirality, the energy position of the first peak decreases with increasing diameter, e.g., the (11,8), (9,9), and (10,7) nanotubes.

The JDOS of the semiconducting carbon nanotubes are shown in Fig. 1(b). They are vanishing at $\omega<E_g$, owing to the absence of the linear subbands at $E_F=0$. The parabolic subband of $\kappa_x=-2/3d$ or $2/3d$ induces the first peak at $\omega_1=E_g\simeq 2\gamma_0 b/d$. The semiconducting nanotubes do not exhibit the neighboring two-peak structure as shown by the metallic nanotubes [Fig. 1(a)]. For the semiconducting carbon nanotubes with $-30°\leqslant\theta\leqslant-20°$, the second peak due to the subband of $\kappa_x=-4/3d$ or $4/3d$ occurs at $\omega_2\simeq 2\omega_1$, e.g., the (10,9), (11,7), and (9,8) nanotubes. A regular energy difference between the first peak and the second peak could be utilized to determine the preferred chirality in a nanotube bundle.[10] On the other hand, for the semiconducting nanotubes with $-10°\leqslant\theta\leqslant 0°$, the energy position of the second peak does not decrease with the nanotube diameter, e.g., the (14,1) and (14,0) nanotubes. This special result is easily identified from the $\kappa_x^2$ and $\kappa_x^3\cos 3\theta$ terms in Eq. (3). In short, there are several important differences in the low-energy JDOS for metallic and semiconducting nanotubes, or for carbon nanotubes close to zigzag chirality and armchair chirality. They include the peak structures, the peak positions, and the dependence of peaks on the nanotube geometry.

The above-mentioned features of the $\pi$-band structure will be directly reflected in optical excitations. At $T=0$, electrons are excited from the occupied $\pi$ subbands to the unoccupied $\pi^*$ subbands, i.e., they only exhibit inter-$\pi$-band excitations. The optical absorption function of the $(m,n)$ carbon nanotubes is given by[19]

$$A(\omega;d,\theta)=\frac{8e^2\omega^2}{\sqrt{3}(d+I_c)^2}\sum_{k_x,k_x'}\int_{1\text{st BZ}}\frac{dk_y}{2\pi}\times\frac{\left|\left\langle\Psi^c(k_x',k_y)\left|\frac{\hat{\mathbf{E}}\cdot\mathbf{P}}{m_e}\right|\Psi^v(k_x,k_y)\right\rangle\right|^2}{\omega_{vc}^2(k_x,k_x',k_y)}\times\left(\frac{\Gamma}{[\omega-\omega_{vc}(k_x,k_x',k_y)]^2+\Gamma^2}-\frac{\Gamma}{[\omega+\omega_{vc}(k_x,k_x',k_y)]^2+\Gamma^2}\right).\tag{5}$$

$I_c$ $(=3.4\,\text{Å})$ is the intertube distance. $\omega_{vc}(k_x,k_x',k_y)=E^c(k_x',k_y)-E^v(k_x,k_y)$ is the inter-$\pi$-band excitation energy. The square of the velocity matrix element in Eq. (5) is evaluated within the gradient approximation.[16] There exist selection rules for the optical excitations, that greatly simplify the calculations. One is that $\Delta k_y=0$ in Eq. (5) (or $\Delta\kappa_y=0$), which follows from the fact that for photons in the long-wavelength limit the initial- and final-state wave vectors are the same. On the other hand, the selection rules of the angular momentum depend on the polarization direction. For $\mathbf{E}_\parallel$, it satisfies $\Delta J=0$ (or $\Delta\kappa_x=0$). This means that only the vertical transitions from the $\pi$ to the $\pi^*$ subbands of the same $J$'s are allowed. But for $\mathbf{E}_\perp$, allowed excitations are restricted to subbands that satisfy $\Delta J=\pm 1$ (or $\Delta\kappa_x=\pm 2/d$). The reason is that the matrix element $\hat{\mathbf{E}}\cdot\mathbf{P}\propto(\sin\alpha)P_\alpha$, where $\alpha$ is the azimuthal angle. Expressing $\sin\alpha=(e^{i\alpha}-e^{-i\alpha})/2i$, one readily sees that the selection rule follows. In this case, electrons in the $\pi$ subband of $J$ are excited to the $\pi^*$ subband of $J\pm 1$. The two excitation channels, $\Delta J=\pm 1$, make the same contributions to optical excitations. It only needs to be carried out for one excitation channel, e.g., for $\Delta J=1$.

In general, a carbon nanotube bundle is made up of single-wall carbon nanotubes with different diameters and chiral angles. The optical excitations of a nanotube bundle is the superposition of those of different carbon nanotubes. The ensemble average of the optical absorption function is $A(\omega)=\langle A(\omega;d_i,\theta_i)\rangle_{av}$. The imaginary part of the dielectric function[19] could be directly evaluated from the optical absorption function by the relation $\epsilon_2(\omega)=2\pi A(\omega)/\omega^2$. The real part of the dielectric function is subsequently found by means of the Kramers-Kronig relation

$$\epsilon_1(\omega)-\epsilon_0=\frac{-1}{\pi}\int_{-\infty}^{\infty}\epsilon_2(\omega')\text{P}\left(\frac{1}{\omega-\omega'}\right)d\omega',\tag{6}$$

where $\epsilon_0$ (=2.4 (Ref. 20) is the background dielectric constant. Loss function and reflectance are, respectively, calculated from $\mathrm{Im}[-1/\epsilon]$ and $R(\omega)=|1-\sqrt{\epsilon(\omega)}|^2/|1+\sqrt{\epsilon(\omega)}|^2$.

### III. THE CALCULATED OPTICAL SPECTRA

Equations (5) and (6) are used to calculate the optical absorption function, the dielectric function, the loss function, and the reflectance. The distribution of diameter and chiral angle in a nanotube bundle is needed for the calculations of the ensemble average of optical properties. It is mainly determined by synthesis temperature and catalysts.[9–11] A highly uniform carbon nanotube bundle could be produced. However, the real distribution of the nanotube geometry is not known up to now. Here the single-walled carbon nanotubes are assumed to group around the $(m,m)$ armchair nanotube[10,11] [or the $(m,0)$ zigzag nanotube]. A $(m,m)[(m,0)]$ carbon nanotube has the diameter $d_0=3mb/\pi$ $[d_0=\sqrt{3}mb/\pi]$. The diameter and the chiral angle are, respectively, confined to $d_0\pm\Delta d$ and $-30°\leqslant\theta\leqslant-20°$ $(-10°\leqslant\theta\leqslant0°$; for details see Fig. 4 in Ref. 11). The maximum distribution width $\Delta d$ does not significantly modify the optical spectra [Fig. 2(a)]. The number of single-wall carbon nanotubes with diameter $d$ in a bundle is proportional to the Lorentzian distribution $d_c/[(d-d_0)^2+d_c^2/4]$ or the Gaussian distribution $\exp[-2(d-d_0)^2/d_c^2]$. The calculated results are almost the same for these two kinds of distributions. The Lorentzian distribution is taken in the calculations.

We first study the optical absorption in the $\mathbf{E}_\parallel$ case for the (9,9) nanotube bundle with $-30°\leqslant\theta\leqslant-20°$ and $\Delta d=0.07$ nm. This bundle is close to that produced at $T=1050\,°\mathrm{C}$ by catalyst NiCo [Fig. 3(b) in Ref. 10]. There are nine kinds of single-wall carbon nanotubes in a nanotube bundle.[11] They include six semiconducting nanotubes [(9,8), (11,6), (10,8), (11,7), (10,9); (12,7)] and three metallic nanotubes [(10,7), (9,9); (11,8)]. $d\sim1.15$ nm for the (9,8), (10,7); (11,6) nanotubes. $d\sim1.22$ nm for the (9,9), (10,8); (11,7) nanotubes. $d\sim1.29$ nm for the (10,9), (11,8); (12,7) nanotubes. $A^\parallel$, as shown by the light solid curve in Fig. 2(a), is due to the inter-$\pi$-band $e$-$h$ excitations from the $\Psi^v(J,k_y)$ state to the $\Psi^c(J,k_y)$ state. At an energy $\omega$, which corresponds to vertical optical excitations near the band edge, the number of such excitation channels is very large. JDOS exhibits a sharp peak (Fig. 1), and so does $A^\parallel$. A carbon nanotube bundle is made up of different carbon nanotubes. Consequently, there are three main absorption bands, and several subpeaks or shoulders exist in each absorption band. The semiconducting (metallic) nanotubes cause the first and the second absorption bands (the third absorption band), as indicated from the comparison between Fig. 1 and Fig. 2(a). The velocity matrix elements of the linear subbands vanish [Eq. (5)]; therefore, the metallic nanotubes do not exhibit finite absorption spectrum at very low frequency. The optical threshold excitations are related to the semiconducting nanotubes, and the threshold excitation frequencies are their energy gaps. The optical absorption spectrum is somewhat modified with an increase of the distribution width of diameter, e.g., $A^\parallel$ at $\Delta d=0.14$ nm (the light dashed curve). There exist additional subpeaks, which are far away from the central peaks of absorption bands (denoted by arrows). $A^\parallel$ at $\Delta d=0.14$ nm is found to be almost the same as that at $\Delta d\geqslant0.21$ nm. Generally speaking, the effect of $\Delta d$ on the optical spectra is weak.

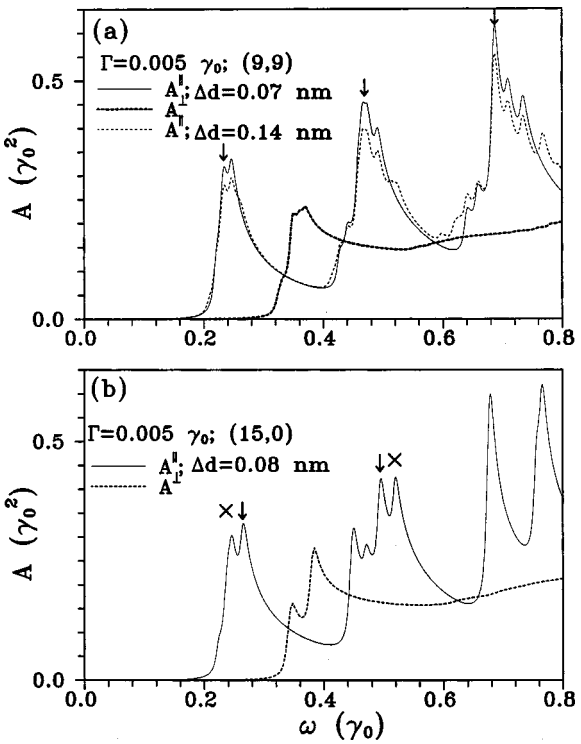


FIG. 2. The optical absorption functions are calculated at $\Gamma=0.005\gamma_0$ for (a) the (9,9) nanotube bundle with $\Delta d=0.07$ nm and (b) the (15,0) nanotube bundle with $\Delta d=0.08$ nm. The light solid curve and the heavy dashed curve are the results for the parallel and perpendicular polarizations directions, respectively. Also shown in (a) for comparison is $A^\parallel$ at $\Delta d=0.14$ nm. The arrows in (a) points at the central peak in each absorption band. The arrows and crosses in (b), respectively, correspond to the subpeaks induced by the (14,0) and (14,1) nanotubes.

The subpeaks or shoulders in absorption bands have three important features. First, the semiconducting (10,8) and (11,7) nanotubes induce the central peaks in the first and the second absorption bands, and the metallic (9, 9) nanotube leads to that in the third absorption band. These three peaks, respectively, occur at $\omega_1\simeq2\gamma_0b/d_0$, $\omega_2\simeq4\gamma_0b/d_0$, and $\omega_3\simeq6\gamma_0b/d_0$ [Eq. (3)]. This result suggests that we could infer the mean diameter of the nanotube bundle or the value of $\gamma_0$ from the energy positions of the central peaks. Second, for the first absorption band, the energy difference between the central peak and the neighboring peak (or shoulder) is $E_{D1}\simeq\omega_1\Delta d/d_0$. The energy difference becomes double for the second absorption band, i.e., $E_{D2}\simeq\omega_2\Delta d/d_0$. There is a simple corresponding relation for the subpeaks in the first and the second absorption bands. Finally, the first and the third absorption bands, respectively, have the narrowest and the widest distribution widths. Compared with the first and the second absorption bands, the third absorption band exhibits more subpeaks. The main reason is that the nonarmchair metallic nanotubes, the (10,7) and (11,8) nanotubes, exhibit the neighboring two-peak structure [Fig. 1(a)].

The above-mentioned features of $A^\parallel$ could essentially explain the measured absorption spectra.[9,10] They include the three absorption bands at $\omega<0.8\gamma_0$,[9,10] the subpeaks (or

shoulders) and the central peak in each absorption band,[10] the corresponding subpeak positions in the first and the second absorption bands,[10] and the widest frequency range for the third absorption band.[10] The consistency means that the single-walled carbon nanotubes in a nanotube bundle should belong to carbon nanotubes close to armchair chirality, but not zigzag chirality. It is also useful in determining the value of the resonance integral. Kataura *et al.*[9] (Jost *et al.*[10]) make pure single-wall carbon nanotubes by using catalyst NiY (NiCo) at $T=1200\,^{\circ}\mathrm{C}$ ($1050\,^{\circ}\mathrm{C}$). The mean diameter is $d_0=1.36\,\mathrm{nm}$ (1.22 nm) The central peaks in three absorption bands, respectively, occur at 0.68, 1.2, and 1.7 eV (0.77, 1.41, and 2.04 eV). A comparison between these energy positions and the theoretical predictions $(\omega_1,\omega_2;\omega_3)$ yields a value of $\gamma_0=3.0\pm0.2\,\mathrm{eV}$ ($\gamma_0=3.1\pm0.2\,\mathrm{eV}$).

The nanotube chirality has a strong effect on the optical absorption spectra. $A^{\|}$ of the (15, 0) nanotube bundle with $\Delta d=0.08\,\mathrm{nm}$ is shown in Fig. 2(b). This bundle has eight kinds of single-wall carbon nanotubes. It includes[11] six semiconducting nanotubes [(14,0), (13,2), (14,1), (15,1), (14,3); (16,0)] and two metallic nanotubes [(15,0); (14,2)]. There are several important differences between the (15, 0) nanotube bundle and the (9,9) nanotubes bundle [Fig. 2(a)] in $A^{\|}$. The former also exhibits three absorption bands. However, it is difficult to find the central peak in each absorption band. The corresponding relation between the subpeaks in the first and the second absorption bands is absent. For example, the (14, 0) nanotube (arrows) is larger than the (14, 1) nanotube (crosses), while the energy positions of the subpeaks are not inversely proportional to diameter [see also Fig. 1(b)]. Moreover, the third absorption band corresponds to two prominent peaks [Fig. 1(a)]. That the nonlinear $\kappa_x^3\cos 3\theta$ term in Eq. (3) is very important for carbon nanotubes with small $\theta$ could explain the above-mentioned results. Apparently, the optical absorption spectra shown by carbon nanotubes close to zizag chirality are not consistent with the experimental measurements.[10,11]

The structure anisotropy of the nanotube bundle is directly reflected in the optical spectra. $A^{\perp}$ in the $\mathbf{E}_{\perp}$ case quite differs from $A^{\|}$ in the $\mathbf{E}_{\|}$ case, as shown in Figs. 2(b) and 2(a). The differences include the spectral intensity, the absorption bands, and the threshold excitations. $A^{\perp}$ is weaker than $A^{\|}$, since the optical transition probability of the former is about half of that of the latter [Eq. (5)]. $A^{\perp}$ only exhibits one absorption band, which comes from semiconducting and metallic carbon nanotubes. On the other hand, $A^{\|}$ exhibits three absorption bands, which, respectively, correspond to semiconducting and metallic nanotubes. Whether there are peak structures in the absorption spectrum depends on the JDOS and velocity matrix element in Eq. (5). The optical matrix elements of the edge states in the $\mathbf{E}_{\perp}$ case are found to be nonvanishing only for the threshold excitations. For metallic (semiconducting) nanotubes, such excitations are caused by the linear (parabolic) subband of $\kappa_x=0$ [$\kappa_x=2/3d$ or $-2/3d$ in Eq. (3)] and the parabolic subband of $\kappa_x=2/d$ or $-2/d$ ($\kappa_x=-4/3d$ or $4/3d$). Consequently, the threshold excitation frequency is higher in the $\mathbf{E}_{\perp}$ case.

Figure 3(a) and 3(b) present the dielectric functions for the (9,9) and (15,0) nanotube bundles, respectively. The imaginary part of the dielectric function is proportional to the optical absorption function. They exhibit similar peak structures at the same energies. The real $[\epsilon_1(\omega)]$ and the imaginary $[\epsilon_2(\omega)]$ parts of the dielectric function satisfy the Kramers-Kronig relation. When $\epsilon_2$ is divergent in $1/\sqrt{\omega-\omega_i}$ form at $\Gamma=0$, $\epsilon_1$ diverges in reverse $1/\sqrt{\omega_i-\omega}$ form. These divergent structures are broadened at finite $\Gamma$. Each singular structure is replaced by the peak structure and the dip structure for $\epsilon_1$ (the peak structure and the step structure for $\epsilon_2$). Clearly, $\epsilon_1^{\|}$ (the heavy dashed curves) might have zeros or be very small in the right-hand neighborhood of the dip structures. The special $\epsilon_1$ will make the loss spectrum exhibit prominent peaks [Figs. 4(a) and 4(b)]. Such peaks are associated with inter-$\pi$-band collective excitations or plasmons. But on the other hand, the dip structures in $\epsilon_1^{\perp}$ (the light dashed curves) are less obvious. They do not lead to the vanishing $\epsilon_1$ and thus the pronounced peaks in the loss spectrum.

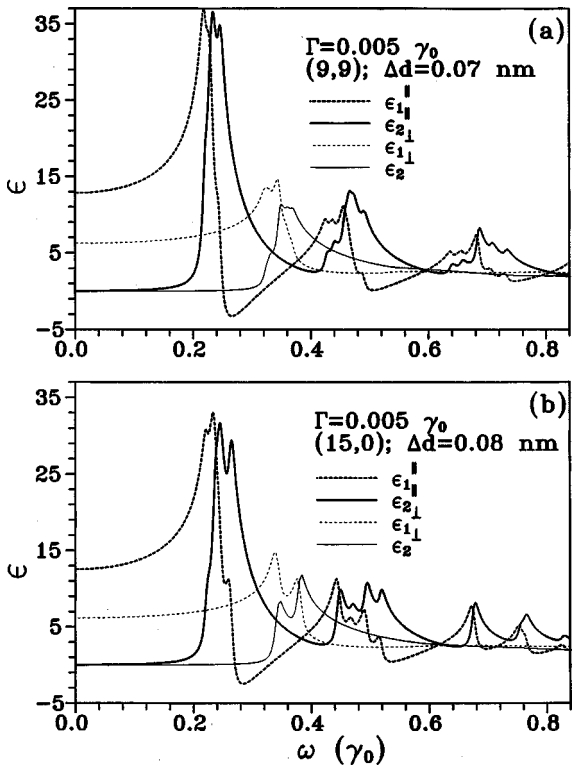


FIG. 3. The real ($\epsilon_1$) and the imaginary ($\epsilon_2$) parts of the dielectric functions are calculated at $\Gamma=0.005\gamma_0$ for (a) the (9,9) nanotubes bundle with $\Delta d=0.07\,\mathrm{nm}$ and (b) the (15,0) nanotube bundle with $\Delta d=0.08\,\mathrm{nm}$.

The loss functions are important in understanding plasmons and single-particle excitations. They are shown in Figs. 4(a) and 4(b) for the (9,9) and (15,0) nanotube bundles, respectively. The loss functions for $\mathbf{E}^{\|}$ exhibit three or four prominent peaks and several subpeaks (the solid curves). However, the former are absent in the $\mathbf{E}_{\perp}$ case (the dashed curves). The prominent peaks and the subpeaks are, respectively, attributed to the inter-$\pi$-band plasmons and $e$-$h$ excitations. The first and the second plasmon peaks (the other plasmon peaks) are caused by the semiconducting (metallic) nanotubes. The subpeak structures are similar to those found in the optical absorption function. The plasmon frequencies are higher than the single-particle excitation energies. Furthermore, there is no simple relation between the plasmon

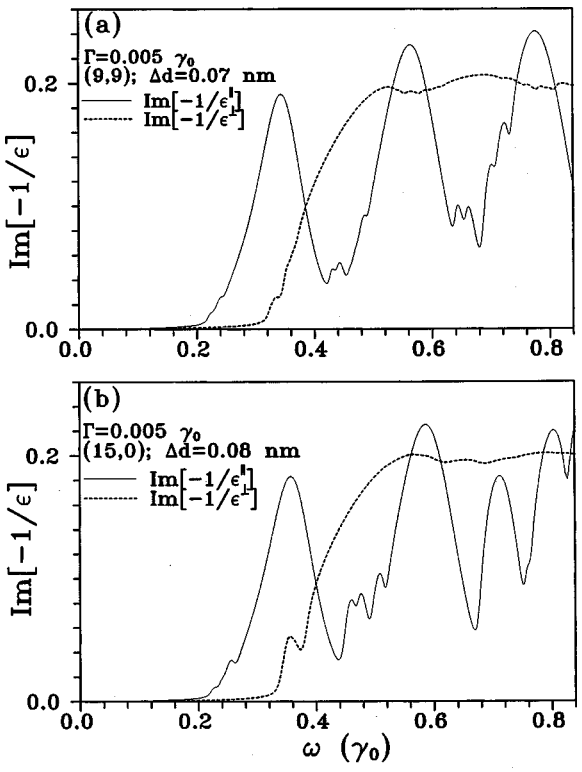


FIG. 4. (a) The loss functions are calculated at $\Gamma = 0.005\gamma_0$ for the (9,9) nanotube bundle with $\Delta d = 0.07$ nm. (b) Same plot as (a), but shown for the (15,0) nanotube bundle with $\Delta d = 0.08$ nm.

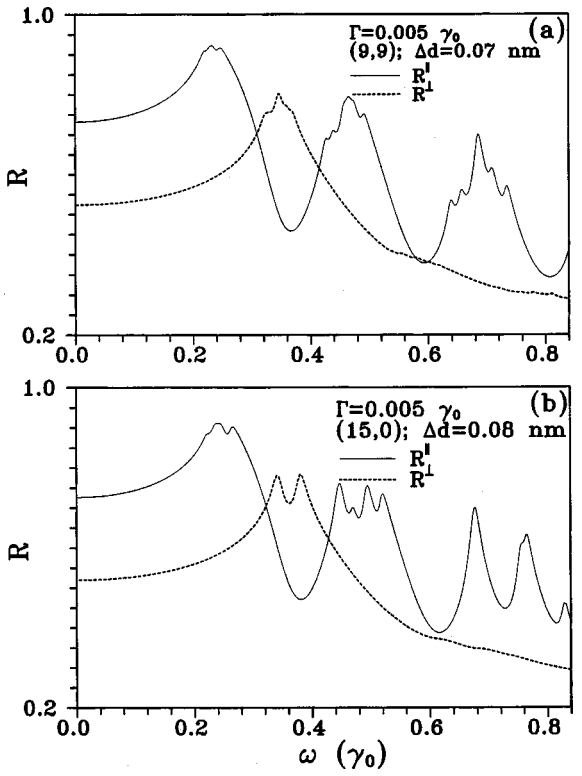


FIG. 5. The reflectance spectra are shown at $\Gamma = 0.005\gamma_0$ for (a) the (9,9) nanotube bundle with $\Delta d = 0.07$ nm and (b) the (15,0) nanotube bundle with $\Delta d = 0.08$ nm.

frequencies and the nanotube diameter. The plasmon peaks are thus expected to be useless for the determination of the nanotube distribution in a nanotube bundle. The inter-$\pi$-band plasmon peaks in single-wall carbon nanotube bundles have been observed with EELS.[11] The calculated results in the $\mathbf{E}_{\|}$ case could account for the origin of these plasmons.

The reflectance spectra are, respectively, shown in Figs. 5(a) and 5(b) for the (9,9) and (15,0) nanotube bundles. When the optical excitations come from the edge states of the $\pi$ subbands, the dielectric function exhibits sharp peaks. Both reflectance spectra and absorption spectra behave so; that is, they have similar peak structures. For example, there are three main peak structures in $R^{\|}(\omega)$ (Fig. 5) and $A^{\|}(\omega)$ (Fig. 2). Each subpeak is due to the $e$-$h$ excitations, and the energy position is related to the nanotube geometry. The peak structures in $R^{\|}(\omega)$, as discussed earlier for $A^{\|}(\omega)$, could be used to identify the preferred nanotube geometry in a nanotube bundle. $R^{\|}(\omega)$ are local maxima at peak positions and then rapidly drops to local minima. The clear plasmon edges occur at plasmon frequencies where the inter-$\pi$-band plasmons are located. The reflectance spectra could directly display the characteristics of the single-particle and collective excitations.

## IV. CONCLUDING REMARKS

In this work, the low-frequency optical properties of single-wall carbon nanotube bundles are studied within the gradient approximation.[16] The nanotube geometry and the polarization direction significantly affect the optical absorption function, the dielectric function, the loss function, and the reflectance. The absorption spectra and the reflectance spectra are predicted to be useful in determining the nanotube geometry in a nanotube bundle, but not the loss spectra. The calculated results could provide a reasonable explanation for the measured absorption spectra[10,11] and loss spectra.[15]

The optical absorption functions for $\mathbf{E}_{\|}$ and $\mathbf{E}_{\perp}$, respectively, exhibit three absorption bands and one absorption band. For $A^{\|}$, the semiconducting (metallic) carbon nanotubes induce the first and the second absorption bands (the third absorption band). However, the only absorption band in $A^{\perp}$ comes from all carbon nanotubes. There are several subpeaks in each absorption band. For carbon nanotubes close to armchair chirality, the energy position of the central peak is inversely proportional to the nanotube diameter. Furthermore, there exists a corresponding relation for the subpeaks in the first and the second absorption bands. On the other hand, these two simple relations are absent for carbon nanotubes close to zigzag chirality. The dielectric function and the reflectance vary as the optical absorption function. That is to say, their peak structures are due to the single-particle excitations, and they are related to the nanotube geometry. Such peaks are in great contrast with the pronounced peaks in the loss function, since the latter correspond to the collective excitations. The inter-$\pi$-band plasmons also lead to clear plasmon edges in the reflectance spectra.

## ACKNOWLEDGMENT

This work was supported in part by the National Science Council of Taiwan, the Republic of China, under the Grant No. NSC 89-2112-M-006-011.

[1] S. Iijima, Nature (London) **354**, 56 (1991).
[2] J. W. Mintwire, B. I. Dunlap, and C. T. White, Phys. Rev. Lett. **68**, 631 (1992).
[3] J. W. Mintwire and C. T. White, Phys. Rev. Lett. **81**, 2506 (1998).
[4] C. T. White and T. N. Todorov, Nature (London) **393**, 240 (1998).
[5] N. Hamada, S. I. Sawada, and A. Oshiyama, Phys. Rev. Lett. **68**, 1579 (1992).
[6] R. Saito, M. Fujita, G. Dresselhaus, and M. S. Dresselhaus, Appl. Phys. Lett. **60**, 2204 (1992); Phys. Rev. B **46**, 1804 (1992).
[7] J.-C. Charlier and Ph. Lambin, Phys. Rev. B **57**, 15 037 (1998).
[8] A. Thess, R. Lee, P. Nikolaev, H. Dai, P. Petit, J. Robert, C. Xu, Y. H. Lee, S. G. Kim, A. G. Rinzler, D. T. Colbert, G. E. Scuseria, D. Tomanek, J. E. Fischer, and R. E. Smalley, Science **273**, 483 (1996).
[9] H. Kataura, Y. Kumazawa, Y. Maniwa, I. Umezu, S. Suzuki, Y. Ohtsuka, and Y. Achiba, Synth. Met. **103**, 2555 (1999).
[10] O. Jost, A. A. Gorbunov, W. Pompe, T. Pichler, R. Friedlein, M. Knupfer, M. Reibold, H.-D. Bauer, L. Dunsch, M. S. Golden, and J. Fink, Appl. Phys. Lett. **75**, 2217 (1999).
[11] For the nanotube distribution in a bundle see (Fig. 4) S. Bandow, S. Asaka, Y. Saito, A. M. Rao, L. Grigorian, E. Richter, and P. C. Eklund, Phys. Rev. Lett. **80**, 3779 (1998).
[12] A. M. Rao, E. Richter, S. Bandow, B. Chase, P. C. Eklund, K. A. Williams, S. Fang, K. R. Subbaswamy, M. Menon, A. Thess, R. E. Smalley, G. Dresselhaus, and M. S. Dresselhaus, Science **275**, 187 (1997).
[13] D. Bernaerts, A. Zettl, N. G. Chopra, A. Thess, and R. E. Smalley, Solid State Commun. **105**, 145 (1998).
[14] J. M. Cowley, P. Nikolaev, A. Thess, and R. E. Smalley, Chem. Phys. Lett. **265**, 379 (1997).
[15] T. Pichler, M. Knupfer, M. S. Golden, J. Fink, A. Rinzler, and R. E. Smalley, Phys. Rev. Lett. **80**, 4729 (1998).
[16] L. G. Johnson and G. Dresselhaus, Phys. Rev. B **7**, 2275 (1973).
[17] For the details of the nanotube geometry and the $\pi$-band structure see M. F. Lin and K. W.-K. Shung, Phys. Rev. B **52**, 8423 (1995).
[18] P. R. Wallace, Phys. Rev. **71**, 622 (1947).
[19] G. D. Mahan, *Many-Particle Physics* (Plenum, New York, 1990).
[20] E. A. Taft and H. R. Philipp, Phys. Rev. **138**, A197 (1965).